ISSN 1027-4510, Journal of Surface Investigation: X-ray, Synchrotron and Neutron Techniques, 2021, Vol. 15, No. 4, pp. 752–758. © Pleiades Publishing, Ltd., 2021.
Russian Text © The Author(s), 2021, published in Poverkhnost', 2021, No. 7, pp. 96–103.

Effect of Lithium on the Structural-Phase State of Rapidly Solidified Al–Mg–Li Alloy During Heat Treatment

I. A. Stoliar[a], *, V. G. Shepelevich[a], E. Wendler[b], and I. I. Tashlykova-Bushkevich[c], **

[a] *Belarusian State University, Minsk, 220050 Belarus*
[b] *Friedrich Schiller University, Jena, 07743 Germany*
[c] *Belarusian State University of Informatics and Radioelectronics, Minsk, 220013 Belarus*
**e-mail: uyluana@gmail.com*
***e-mail: iya.itb@bsuir.by*

Received December 14, 2020; revised January 24, 2021; accepted January 28, 2021

Abstract—The effect of lithium on the structural-phase state of aerospace aluminum alloy 1421 of the Al–Mg–Li system prepared by rapid solidification is studied. Analysis of the composition of the surface layers of alloy samples carried out by means of nuclear reaction analysis establishes that lithium diffuses to the surface at elevated treatment temperatures and its concentration in a thin surface layer (0.1 μm) reaches 38 at %, which is 4.8 times higher than the calculated Li content in the alloy. By measuring the microhardness, strengthening of the samples is determined upon isothermal annealing at a temperature of 400°C, which is caused by the precipitation of metastable lithium-containing phases. The results of X-ray diffraction analysis indicate an increase in the fraction of Li_2O_2 peroxide on the foil surface upon annealing.

Keywords: rapid solidification, Al–Mg–Li–Sc–Zr alloy, phase composition, nuclear-reaction analysis, microhardness

DOI: 10.1134/S1027451021040194

INTRODUCTION

Currently, there is increased research interest in aluminum-magnesium-lithium alloys. The production of lithium, which is the lightest metal, is constantly increasing as it is of great importance in the development of modern technology. The priority of studying alloys of this group is largely determined by their use in the aerospace industry, since the addition of lithium to aluminum provides an increased modulus of elasticity and reduced density, allowing a reduction in the weight of aircraft structures [1, 2]. The properties of materials are influenced by numerous factors, such as dispersion and imperfection of the microstructure, chemical composition, etc. On the one hand, aluminum alloys with well-studied mechanical properties are obtained in industry using a variety of traditional casting methods. On the other hand, technologies, which allow the typical melting cooling rate (about 10^2 K/s) of most methods of obtaining microcrystalline alloys to be exceeded, are of scientific and practical interest. They allow significant modification of the structure, thus improving the physical, corrosion, and technological properties of materials based on aluminum [3]. In particular, high-speed crystallization techniques (centrifugal quenching, spinning, atomization, etc.), providing melt cooling rates on the order of 10^6 K/s and higher, allow materials to be obtained characterized by a greater degree of homogeneity and uniformity (phase and structural), expanding the application areas of the developed alloys.

The aim of this work is to study the effect of lithium on the structural-phase state of the rapidly solidified industrial alloy 1421 of the Al–Mg–Li–Sc–Zr system during heat treatment. Lithium alloyed aluminum alloys can be hardened by heat treatment due to the variable solubility of lithium and other components in solid aluminum. Therefore, the choice of annealing temperatures in this work is based on previously obtained results on the temperature ranges of the maximum hardening of rapidly solidified foils of a given alloy upon isochronous annealing [4]. The relevance of studying Al–Mg–Li alloys using nuclear reaction analysis (NRA) is due to the difficulty of determining the content and distribution of lithium ($Z = 3$) in the surface layers of samples using direct methods of analysis. One of the advantages of this nondestructive nuclear-physical method is the unique possibility of the direct detection and construction of concentration profiles of light elements in a target [5, 6], while this problem cannot be solved using X-ray microanalysis. Scanning electron microscopes additionally equipped with X-ray spectrometers can record the characteristic X-ray radiation of chemical elements of a sample

excited by probe electrons only starting with beryllium ($Z = 4$). Determination of the impurity distribution over the depth of the material by the NRA is based on the dependence of the energy losses of charged particles emitted in nuclear reactions on the depth of analysis. In the present study, the use of NRA made it possible to study elemental-structural changes in the near-surface layers and at the depth of rapidly solidified samples during heat treatment. Additionally, the phase composition of the annealed foils is studied by X-ray diffraction analysis, and the change in the microhardness of the samples during isothermal annealing was also determined.

EXPERIMENTAL

Foils of industrial aluminum alloy 1421 (Al (5.8 at %)–Mg (8.1 at %)–Li (0.03 at %)–Zr (0.11 at %)–Sc) were obtained from the liquid phase by one-sided cooling on the internal surface of a copper cylinder. The rotating speed of the cylinder with a diameter of 20 cm was 1500 rpm. Foils with a thickness of 40–80 μm were examined. The cooling rate of the melt was about 10^6 K/s [7]. When studying the effect of the annealing temperature on the structural-phase composition and microhardness of the foils, the samples were fixed at each temperature in the middle between six glass slides (the thickness of each slide is about 2 mm) to ensure slow heating and cooling of the foil during the experiments at a rate not exceeding 10 deg/s.

The NRA method was used to study both 1421 alloy surfaces of freshly quenched and annealed at $T =$ 380°C for 1 h foils. The surface marked as *A* is in contact with the substrate and the surface *B* is in contact with air. To identify lithium and measure its distribution profiles in the samples, the ^{7}Li(p,α)^{4}He nuclear reaction at a proton energy of 1.4 MeV at a JULIA tandentron (3 MV) accelerator (Jena University Laboratory for Ion Acceleration) was used. Protons and α particles scattered at the sample because of the (p, α) reaction were recorded with a detector with an energy resolution of 15 keV, set at a backscattering angle of $\theta = 170°$ to the direction of the accelerated proton beam.

Information on the composition of the studied samples was obtained based on processing of the energy spectra of scattered particles using the SIMNRA computer program [8], in which, the coincidence of the model and experimentally observed spectra was achieved within the limits of statistical measurement error by varying the elemental composition, the number, and thickness of layers of the model structure. To simulate some of the spectra corresponding to backscattered protons, data on the non-Rutherford cross sections were taken from the IBANDL database [9] and from experimental data for Li [10], C [11], O, and Al [12]. The cross section for the nuclear reaction of protons with Li atoms was taken from [13]. Additionally, the nuclear reaction of protons with Al atoms was taken into account according to [14]. As a reference spectrum obtained under the same conditions and geometry as in the present experiments, the NRA spectrum of a lithium-niobate sample ($LiNbO_3$) with a known lithium content of 20.0 at % was used [15]. The error in determining the lithium concentration by the NRA method was from 5 to 11%.

Since in SIMNRA the thickness of the layers of the model structure h_n is determined as at/cm^2, the conversion of the layer thickness to the metric scale h was performed according to the formula [6]:

$$h = h_n/n_0,$$

where n_0 is the atomic density of the aluminum alloy 1421, assumed equal to the density of aluminum (6.03×10^{22} at cm^{-3}). Thus, the depth of NRA analysis for the 1421 alloy foil was about 22 μm.

The X-ray diffraction study of freshly hardened foils and foils annealed at 400°C for 1 h was carried out on a Rigaku Ultima IV diffractometer using CuK_α radiation. The phases were identified using the ICCD PDF-2 (2013) and Materials Project databases [16]. The microhardness of the samples upon isothermal annealing of the foils at a temperature of 400°C for 110 min was measured using an MVD 402 Wolpert Wilson Instruments automatic microhardness tester with a load of 50 g for 30 s. The microhardness measurement error did not exceed 4%.

RESULTS AND DISCUSSION

Typical experimental and model energy spectra of particles obtained upon the irradiation of freshly quenched and annealed foils of the 1421 alloy with accelerated protons are shown in Fig. 1. The spectra of backscattered protons are observed in the energy range up to 1.4 MeV while the spectra of α particles produced in the reaction of ^{7}Li(p,α)^{4}He with ^{7}Li are seen at energies of 5.0 MeV and above. Both parts of the spectra were simulated in SIMNRA simultaneously. The peaks indicated by arrows in the proton backscattering spectra at 800, 1030, 1120, and 1235 keV are due to the presence of Li, C, O, and Al atoms in the samples, respectively. The profiles of the depth distribution of Li atoms in the foils calculated from the NRA spectra are shown in Fig. 2.

For the freshly hardened 1421 alloy foil, the measured spectra of both surfaces are in good agreement with the model spectra. No significant difference was found between the *A* and *B* sides. As an example, Fig. 1a shows the spectrum of the *A* side of the freshly quenched foil. It was found that a thin surface layer of the foils contains carbon (a small peak at an energy of 1030 keV) and oxidized Al, while Li is uniformly distributed over the depth of the foils (up to a depth of

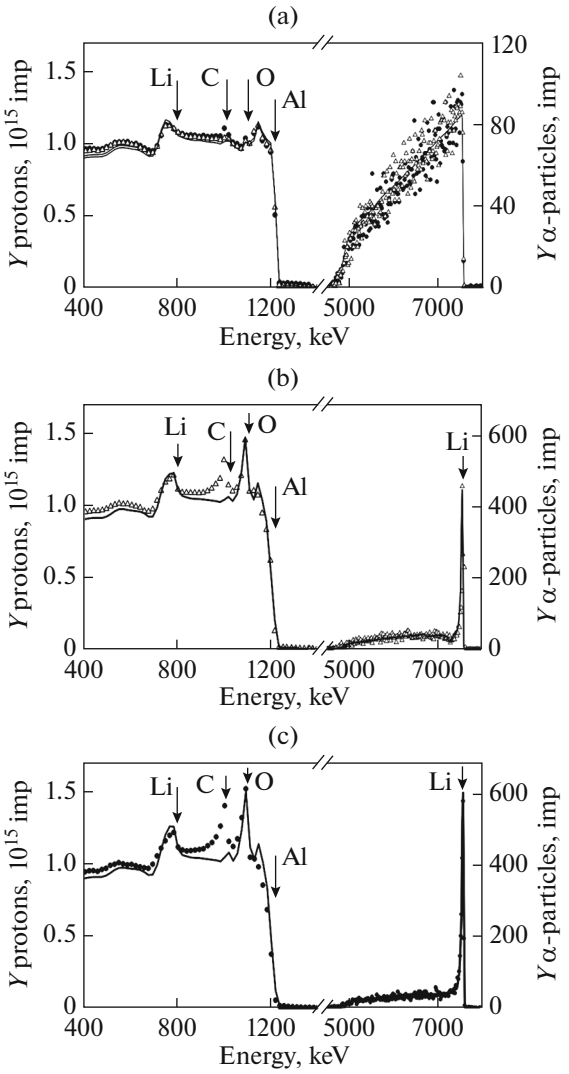

Fig. 1. Typical experimental (symbols) spectra and those simulated using the SIMNRA program (lines) of protons and α particles backscattered at the (a) *A* surface of the freshly quenched 1421 foil and (b, c) *A* and *B* surfaces of the foil annealed at 380°C.

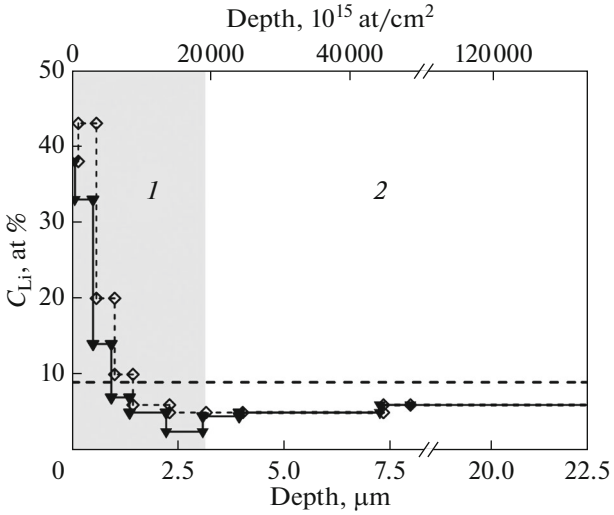

Fig. 2. Distribution of lithium over the *A* surface (solid line) and *B* surface (dashed line) of the 1421 alloy foil annealed at 380°C. The horizontal dashed line defines the lithium distribution profile in the freshly quenched foil. The profile is conventionally divided into two layers with (*1*) uneven and (*2*) even distribution of lithium over the sample depth.

22 μm). It should be noted that using the SIMNRA program it is impossible to determine the Mg content in the samples since the difference in the masses of the Al and Mg atoms is too small. Also, it is not possible to measure the content of Sc and Zr in the surface layer of foils due to the small value of the corresponding signals in the spectra. The average Li concentration in the foils determined by the NRA method is 9 at %, which is 11% higher than the calculated concentration of Li in the alloy (Fig. 2).

The typical energy spectra of backscattered protons and α particles measured after annealing foils of alloy 1421 at 380°C are shown in Figs. 1b, 1c. It was found that in a thin (0.1 μm) surface layer of the *A* and *B* surfaces, the average concentration of Li reaches ~38 at %, which is 4.8 times higher than its calculated content in the alloy. Then the lithium content is reduced to 5.0 at % at a depth of 3 μm (layer *1* in Fig. 2). At a thickness from 3 to 22 μm (layer *2* in Fig. 2), the measured average lithium concentration is 6.0 at %, increasing slightly with depth. Besides, a significant redistribution of Li atoms upon annealing in the direction of the foil surface (right-hand side of Figs. 1b, 1c) is accompanied by a significant increase in the oxygen content on the surface. These results indicate the formation of a Li compound with oxygen on the surface of the samples.

We note that a broad peak is observed in the spectra of backscattered protons in the energy region of ~1.0 MeV, which cannot be modeled (Figs. 1b, 1c). The high-energy edge of this peak cannot be modeled by the backscattering of protons at carbon or nitrogen atoms (the next light element in the periodic table after carbon) on the foil surface. When analyzing the spectra of freshly hardened samples (Fig. 1a), this signal is also detected. Therefore, it can be assumed that the observed signal is the result of an unknown nuclear reaction. Further research is needed to identify the reaction. However, we emphasize that the presence of this peak does not affect the results of determining the Li concentration in foils by NRA, since the depth profile of Li is set by the shape of the measured spectrum of α particles arising from the $^7Li(p,\alpha)^4He$ nuclear reaction. The absolute value of the Li concentration is determined by the yield of *Y* α particles, i.e., the height of the signal in the high-energy region of the spectra (Fig. 1).

Using X-ray diffraction analysis, it was found that lithium peroxide Li_2O_2 is present on the surface of the

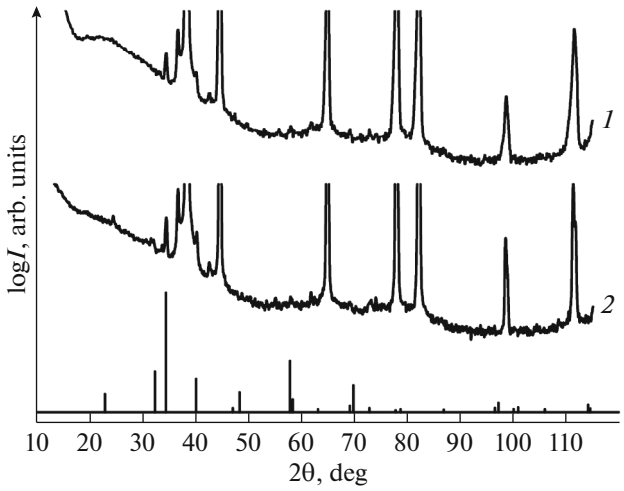

Fig. 3. Diffraction patterns of the foils of 1421 alloy (*1*) freshly quenched and (*2*) annealed at 400°C and the diffraction pattern of lithium peroxide (Li_2O_2, card no. mp-841 [15]).

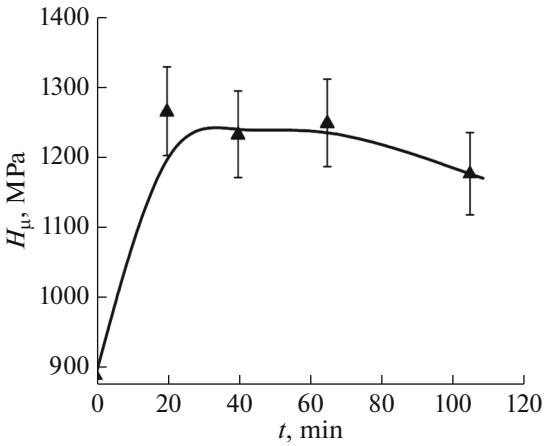

Fig. 4. Microhardness of the 1421 alloy foils depending on the duration of isothermal annealing at 400°C.

freshly quenched samples. Reflections of Li_2O oxide were not recorded in the samples. Figure 3 shows the typical X-ray diffraction patterns of the foils freshly quenched and annealed at 400°C. The lower part of the figure shows a reference diffraction pattern of lithium peroxide, the positions and relative intensities of the reflections of which were taken from the database [16]. Upon heat treatment, with an increase in the annealing temperature, the intensity of the Li_2O_2 lines in the diffraction patterns increases, which indicates an increase in the fraction of lithium peroxide and agrees with the results obtained by NRA (Fig. 3). Additionally, MgO and Al_2O_3 oxides were determined on the surface of the 1421 alloy foils [17].

The study of the dependence of H_μ of the samples of 1421 aluminum alloy on the annealing temperature demonstrates the effect of foil hardening upon annealing at a temperature of 400°C (Fig. 4). At the beginning of annealing, an increase in microhardness to 1.26 GPa is observed after 20 min, which then slightly changes during 110 min of annealing. On average, the value of H_μ is 1200 MPa, which is 33% higher than the microhardness of the initial foil.

The use of aluminum–lithium alloys for the design of aerospace vehicles with a lower mass makes it possible to save fuel, increase the carrying capacity, and improve other characteristics of aircraft. Indeed, each percentage of lithium reduces the density of aluminum by 3%, increases the modulus of elasticity by 6%, and provides a significant effect of hardening of alloys after quenching and artificial aging [2]. The industrial alloy 1421, which belongs to a large group of Al–Mg–Li alloys, is medium strength and is widely used in riveted and welded structures. The required level of alloy strength is mainly determined by the content of Li, Mg, and Sc [18]. It has no analogs abroad since, due to significant difficulties associated with the melting and casting of Al–Mg–Li alloys with rare-earth elements, foreign firms have concentrated their efforts mainly on the development of more technologically advanced AA7075, AA7178, and AA7050 alloys belonging to the Al–Li–Cu, Al–Li–Mg–Cu, and Al–Zn–Mg–Cu systems. However, these alloys have lower density parameters than the 1421 alloy [2].

It is known that materials obtained using ultrafast quenching from the melt are formed in the state of a supersaturated solid solution, which, in turn, leads to more accelerated decomposition of the solid solution compared to cast aluminum alloys with the release of second phases during heat treatment. In practice, isochronous and isothermal annealing is widely used to study the thermal stability of rapidly solidified aluminum alloys. The use of isochronous annealing makes it possible to find the temperature of the onset of changes in the physical properties of the samples. One of the advantages of isothermal annealing in the technology of the production of non-ferrous metals and alloys is the possibility of obtaining a more homogeneous structure since isothermal holding provides temperature equalization in the bulk of the material and all transformations occur at the same degree of supercooling. In particular, the practical interest in studying the temperature effect on the structure of the surface layers of high-alloyed aluminum alloys, widely used in the automotive and aerospace industries, is because their corrosion resistance depends on the chemical and structural heterogeneity of the metal surface. At the same time, the operating mechanisms of hardening in any alloy system depend on the temperature, the degree of applied stress, and the grain size of the alloy. At temperatures close to room temperature, the alloys will deform during slipping (plastic

flow), which is associated with the displacement of dislocations. All anti-slip factors will increase the hardness of the alloy. The movement of dislocations can be hindered by atoms of the solute, precipitates, and/or grain/subgrain boundaries [19]. Therefore, the strategy for increasing the hardness of rapidly solidified alloys is to achieve the optimal combination of solid-solution quenching by increasing the solubility of the alloying element in the solid phase during the formation of a supersaturated solid solution, strengthening with particles of the second phase due to the introduction of a large volume fraction of fine precipitates, and grain-boundary hardening due to a decrease in the grain size [19]. During the annealing of alloys, the coagulation of precipitates, replacement of less stable precipitates with more stable ones, loss of coherence of precipitates, and depletion of the matrix solid solution with the alloying elements lead to a decrease in the hardness of the material [20].

In modern methods of the surface analysis of solids with the deep profiling of impurities, the identification of elements is carried out by the energy of particles and radiation emitted by a material, which is bombarded by electrons, ions, or photons. The NRA method is a nondestructive highly sensitive method for determining the concentration of light impurities in a material, the qualitative composition of which is already known [21]. One of the important advantages of the NRA method is the possibility of studying the depth profiles of the distribution of elements in the surface region of the samples. Hydrogen or helium ions are used as analyzing ions, and secondary particles formed as a result of a nuclear reaction are used as recorded particles.

In this work, the identification of lithium in foils and quantitative analysis were performed by modeling the energy spectra of α particles formed because of a nuclear reaction with $^7Li(p,\alpha)^4He$ protons. The detection of the energy and number of secondary particles made it possible to construct profiles of the lithium distribution over depth. The established regularities of the redistribution of Li because of annealing in rapidly solidified 1421 alloy can be explained by its diffusion from the bulk of the foils to the surface during high-temperature annealing, which leads to decomposition of the supersaturated solid solution and the precipitation of lithium-containing phases. Lithium is an active, easily oxidized element, which, reacts with oxygen on the surface of foils to form lithium peroxide Li_2O_2, which decomposes at a temperature of 450°C [22]. Probably, lithium oxide Li_2O is not identified in the X-ray phase analysis of freshly quenched foils due to segregation on the surface of magnesium samples, the chemical affinity of which for oxygen is higher than that of lithium: $Mg + Li_2O \rightarrow 2Li + MgO$. Although enrichment of the surface of freshly hardened foils of the 1421 alloy with lithium was not found, the segregation inhomogeneity of the foils [23], in particular the enrichment of a thin surface layer of foils with magnesium (20 at %), indicates a significant role of magnesium in the formation of the surface oxide.

According to the results of the segregation of alloying elements in aluminum alloys under high-speed crystallization, the oxide film on the surface of some alloys is similar in composition and structure to the oxide film on pure aluminum, since a number of elements form an enriched layer under the oxide film [24–29]. However, the processes of film growth depend on the method and conditions for implementing ultrafast quenching from the melt. The regularities of the redistribution of lithium as a result of heat treatment in aluminum alloys of the Al–Mg–Li system (the 1421 alloy) have not been sufficiently studied. However, in some works lithium depletion of the surface layer of alloys obtained by the traditional melting and casting method as a result of high-temperature annealing was found [30]. The loosening of Al_2O_3 films due to the presence of lithium and magnesium oxides on the surface of Al–Mg–Li alloys has also been reported [31, 32]. The oxide film formed on the surface of ultrafine-grained 1420 and 1421 alloys by severe plastic deformation after exposure to pulsed laser radiation is reported to consist mainly of magnesium oxides MgO and the compound Li_2CO_3 and is enriched in magnesium and lithium [33, 34]. However, in [33, 34], it is not indicated by which method lithium was identified on the surface of the samples, since the authors refer to the data of X-ray microanalysis, which, as is known, does not allow investigation of this issue. Moreover, there is no quantitative information on the concentration of lithium in the surface region of the samples. Taking into account the foregoing, it can be assumed that the main reasons for the inconsistency of information on the nature of the distribution of lithium over the depth of aluminum alloys are the features of the microstructure of the samples under study, which, as is known, depending on the method of fabrication of the material, as well as the complexity of interpretation [35] of the experimental data obtained using such indirect methods for studying the distribution of lithium in surface layers as electrical resistance [36] and microhardness [37, 38].

It should be noted that the X-ray diffraction analysis of lithium-containing phases of the 1421 alloy foils showed that the foils annealed in the temperature range of 280–450°C contain the S_1 (Al_2LiMg) phase in addition to Li_2O_2 peroxide [39]. The additional comparison of X-ray structural data and the results of studying the annealed foils by scanning electron microscopy, X-ray spectral microanalysis [4, 17, 39], and NRA gives grounds to identify the metastable *X* phase previously found in annealed foils as a Li-containing phase of variable composition $Al(Mg, Sc, Zr, Li)_x$. As noted above, according to some reports, the $Al(Mg, Sc, Zr, Li)_x$ phase was also detected in ultrafine-grained samples of the 1421 alloy obtained in a nonequilibrium state by equal-channel angular press-

ing [40–42]. However, no information has been found on how the processes of precipitation/dissolution of the Al(Mg, Sc, Zr, Li)$_x$ phase affect the mechanical properties of the 1421 alloy. The results of this work are in good agreement with the previously established plateau on the curve of the H_μ dependence on the temperature of isochronous annealing in the range of 340–400°C [4] and indicate that the precipitation of highly dispersed intermetallic S_1 and X phase particles during annealing at about 300°C causes an increase in the microhardness of foils when increasing the annealing temperature to 400°C.

The observed effect of a manifold increase in the Li content on the surface of the annealed foils and the established strengthening of the 1421 alloy foils during high-temperature annealing caused by the precipitation of Li-containing phases, indicates that it is promising to continue the study of structural-phase transformations occurring during heat treatment of the rapidly solidified 1421 alloy for improvement of the physical and mechanical properties of Al–Mg–Li alloys.

CONCLUSIONS

The influence of lithium on the structural-phase state of the rapidly solidified foils made of Al–Mg–Li 1421 alloy under high-temperature annealing was studied using NRA, X-ray diffraction analysis, and microhardness measurements. For the first time, the effect of Li redistribution after annealing at 380°C was discovered. In the surface layer (0.1 μm), the Li concentration is about 38.0 at %, which is 4.8 times higher than its calculated content in the alloy. The difference between the Li concentration on the surface and at the maximum detectable depth (22 μm) of the annealed foils reaches 6.3 times. Lithium diffusing onto the foil surface during high-speed crystallization reacts with oxygen to form lithium peroxide Li_2O_2. The proportion of peroxide increases during heat treatment with an increase in the annealing temperature. Strengthening of the samples by 33% was found upon isothermal annealing at a temperature of 400°C.

REFERENCES

1. T. N. Antipova, A. A. Labutin, and A. Yu. Oleshko, *Quality Management of Technological Processes* (Nauchnyi Konsul'tant, Korolev, 2015), p. 165.
2. T. Dorin, A. Vahid, and J. Lamb, *Fundamentals of Aluminum Metallurgy*, Ed. by R. N. Lumley (Woodhead, Cambridge, 2018).
3. A. M. Kuzei, *Structural Phase Transformations in Rapidly Quenched Aluminum Alloys* (Belaruskaya Navuka, Minsk, 2011) [in Russian].
4. V. G. Shepelevich, I. A. Bushkevich, E. Wendler, and I. I. Tashlykova-Bushkevich, J. Surf. Invest.: X-Ray, Synchrotron Neutron Tech. **13**, 555 (2019). https://doi.org/10.1134/S1027451019030327
5. L. C. Feldman and J. W. Mayer, *Fundamentals of Surface and Thin Film Analysis* (Elsevier, New York, 1986; Mir, Moscow, 1989).
6. C. Jeynes and J. L. Colaux, Analyst **141**, 5944 (2016). https://doi.org/10.1039/c6an01167e
7. I. S. Miroshnichenko, *Quenching from a Liquid State* (Metallurgiya, Moscow, 1982) [in Russian].
8. M. Mayer, *SIMNRA, a Simulation Program for the Analysis of NRA, RBS and ERDA* (Am. Inst. Phys., New York, 1999).
9. IBANDL. https://www-nds.iaea.org/exfor/ibandl.htm.
10. S. Bashkin, Phys. Rev. **84**, 1124 (1951). https://Doi.org/10.1103/PhysRev.84.1124
11. D. Abriola, A. F. Gurbich, M. Kokkoris, A. Lagoyannis, and V. Panneta, Nucl. Instrum. Methods Phys. Res., Sect. B **269**, 2011 (2011). https://doi.org/10.1016/j.nimb.2011.06.002
12. A. F. Gurbich, Nucl. Instrum. Methods Phys. Res., Sect. B **268**, 1703 (2010). https://doi.org/10.1016/j.nimb.2010.02.011
13. W. Wesch, J. Rensberg, M. Schmidt, and E. Wendler, J. Appl. Phys. **126**, 125105 (2019). https://doi.org/10.1063/1.5116667
14. M. A. Abuzeid, F. M. Aly, Y. P. Antoufiev, A. T. Baranik, T. M. Nower, and P. V. Sorokin, Nucl. Phys. **45**, 123 (1963). https://doi.org/10.1016/0029-5582(63)90788-0
15. E. Schmidt, K. Ritter, K. Gartner, and E. Wendler, Nucl. Instrum. Methods Phys. Res., Sect. B **409**, 126 (2017). https://doi.org/10.1016/j.nimb.2017.03.111
16. Materials Project. https://materialsproject.org.
17. I. A. Bushkevich, V. G. Shepelevich, E. Wendler, I. I. Tashlykova-Bushkevich, N. V. Adintsov, and M. V. Kocherga, in *Proceedings of 13th International Conference on Interaction of Radiation with a Solid* (Minsk, 2019), p. 505.
18. V. G. Davydov, L. B. Ber, V. I. Elagin, M. V. Samarina, N. I. Kolobnev, and L. B. Khokhlatova, Tekhnol. Legk. Splavov, No. **1**, 9 (1996).
19. L. A. Davis, S. K. Das, J. C. M. Li, and M. S. Zedalis, Int. J. Rapid Solid **8**, 73 (1994).
20. I. I. Novikov, *Theory of Heat Treatment of Metals* (Metallurgiya, Moscow, 1978) [in Russian].
21. W. A. Lanford, M. Parenti, B. J. Nordell, et al., Nucl. Instrum. Methods Phys. Res., Sect. B **371**, 211 (2016). https://doi.org/10.1016/j.nimb.2015.10.052
22. N. N. Greenwood and A. Earnshaw, *Chemistry of the Elements* (Butterworth-Heinemann, Oxford, 1998).
23. I. A. Bushkevich and V. G. Shepelevich in *Proceedings of 12th International Conference on Interaction of Radiation with a Solid* (Minsk, 2017), p. 211.
24. I. I. Tashlykova-Bushkevich, Vacuum **78**, 529 (2005). https://doi.org/10.1016/J.VACUUM.2005.01.080
25. I. I. Tashlykova-Bushkevich, J. Alloys Compd. **478**, 229 (2009). https://doi.org/10.1016/j.jallcom.2008.12.006
26. V. V. Likutin, A. V. Krainikov, and G. E. Thompson, Fiz. Met. Metalloved. **97**, 58 (2004).
27. A. V. Krainikov, Poroshk. Metall., Nos. **7–8**, 34 (2010).

28. P. Yu. Kikin, V. N. Perevezentsev, and E. E. Rusin, Phys. Met. Metallogr. **118**, 180 (2015).
29. I. I. Tashlykova-Bushkevich, V. G. Shepelevich, M. Amati, L. Gregoratti, and M. Kiskinova, J. Surf. Invest.: X-Ray, Synchrotron Neutron Tech. **14**, 66 (2020).
30. I. N. Fridlyander, V. S. Sandler, and T. I. Nikol'skaya, Metalloved. Term. Obrab. Met., No. 2, 20 (1983).
31. A. I. Vorob'ev, Sb. Ref. Nauchno-Issled. Opytno-Konstrukt. Rabot, Ser. 9:53. Metall. **3** (3), 43 (2007).
32. A. F. Dresvyannikov and M. E. Kolpakov, Vestn. Kazan. Tekhnol. Univ. **19** (9), 36 (2016).
33. P. Yu. Kikin, V. N. Perevezentsev, E. E. Rusin, and N. V. Zemlyakova, Metalloved. Term. Obrab. Met., No. 8, 43 (2012).
34. P. Yu. Kikin, V. N. Perevezentsev, and E. E. Rusin, Phys. Met. Metallogr. **118**, 180 (2015).
35. T. Schoeberl and S. Kumar, J. Alloys Compd. **255**, 135 (1997). https://doi.org/10.1016/S0925-8388(96)02818-6
36. Y. Minamino, T. Yamane, and H. Araki, Metall. Mater. Trans. A **18**, 1536 (1987). https://doi.org/10.1007/BF02646667
37. M. S. Udyavar and E. S. Dwarakadasa, J. Mater. Sci. Lett. **11**, 490 (1992). https://doi.org/10.1007/BF00731114
38. J. M. Papazian and R. L. Schulte, Metall. Mater. Trans. A **21**, 39 (1990). https://doi.org/10.1007/BF02656422
39. I. A. Bushkevich, A. V. Borodyn, Yu. E. Fishkina, and I. I. Tashlykova-Bushkevich in *Proceedings of the VIII International Conference on Actual Problems of Solid State Physics* (Minsk, 2018), Vol. 1, p. 134.
40. Yu. Buranova, V. Kulitskkiy, M. Peterlechner, A. Mogucheva, R. Kaibyshev, S. V. Divinski, and G. Wilde, Acta Mater. **124**, 210 (2017). https://doi.org/10.1016/j.actamat.2016.10.064
41. R. Kaibyshev, K. Shipilova, F. Musin, and Y. Motohashi, Mater. Sci. Technol. **21**, 408 (2005). https://doi.org/10.1179/174328405X36610
42. R. K. Islamgaliev, N. F. Yunusova, R. Z. Valiev, N. K. Tsenev, V. N. Perevezentsev, and T. G. Langdon, Scr. Mater. **49**, 467 (2003). https://doi.org/10.1016/S1359-6462(03)00291-4

Translated by D. Kharitonov